Wave Inversion Technology, Report No. 3, pages 39-49

Inversion by means of kinematic wavefield attributes

P. Majer, G. Höcht, J. Mann, K.-U. Vieth[1]

keywords: *wavefield attributes, cubic splines*

ABSTRACT

We present an inversion method to determine a 2D macro-velocity model by layer stripping. The procedure requires identified primary reflection events in a simulated zero-offset section and kinematic attributes of hypothetical wavefronts. These wavefield attributes are associated with the primary reflection events and can be obtained from the common-reflection-surface stack.

INTRODUCTION

Conventional processing methods only use stacking velocities which are derived from selected common-midpoint (CMP) gathers. However, the stacking velocity does not provide sufficient information to determine an accurate macro-velocity model. In contrast, we present a method that uses kinematic wavefield attributes to compute a layered model with curved interfaces. The procedure requires identified primary reflection events in the zero-offset (ZO) section and the corresponding wavefield attributes R_{NIP},R_N and α. These wavefield attributes are related to the locations and curvatures of interface segments (Hubral, 1983). They are provided by the common-reflection-surface (CRS) stack (Höcht et al., 1999; Jäger et al., 1999). Actually, this inversion method uses the same basic concepts to characterize curved interfaces in laterally inhomogeneous media as the CRS stack. A triplet of these wavefield attributes is associated with a point $P_0 = (x_0, t_0)$ located on a primary reflection event. Here, x_0 denotes the observation point on the surface and t_0 is the zero-offset traveltime. By means of geometrical optics, point P_0 and its wavefield attributes allow to determine the corresponding reflection point in the depth domain by assuming the overburden to be known. Therefore, this implies a layer stripping approach.

[1]**email:** Patrick.Majer@gpi.uni-karlsruhe.de

INVERSION OF THE WAVEFIELD ATTRIBUTES BY GEOMETRICAL OPTICS

To construct the velocity model, we propagate the hypothetical wavefronts characterized by α and the two radii of curvature R_{NIP} and R_N from a surface point x_0 in the direction given by the emergence angle α. We assume a subsurface model with layers of constant velocities separated by continuous smooth interfaces. Knowing the velocity v_0 of the uppermost layer, we successively calculate interface by interface, i. e. in a layer-stripping method.

Let us consider a point $P = (x_0, t_1)$ on the first primary reflection event in the ZO section with its associated attributes α, R_{NIP} and R_N. To calculate the corresponding depth point of the first interface we use the propagation law (Hubral and Krey, 1980) which accounts for the geometrical spreading inside an iso-velocity layer (Figure 1).

$$R_{NIP} = v_0 t_1 \,, \tag{1}$$

$$R_N = v_0 t_1 + R_R \,. \tag{2}$$

Here, R_R denotes the radius of curvature of the reflector at depth point S, which we do not use for further computation. Point S is given by the attributes α and R_{NIP}:

$$S = (x_0 - R_{NIP} \sin \alpha_1, R_{NIP} \cos \alpha_1). \tag{3}$$

All depth points corresponding to the first reflection event serve to construct the first interface by interpolating functions, e. g. cubic splines.

The subsequent reflection event in the ZO section and its wavefield attributes $\tilde{R}_{NIP}$, $\tilde{R}_N$ and $\tilde{\alpha}$ allow to determine the second interface. To locate the depth point corresponding to point $P_2 = (x_0, t_2)$ on this event, we downward propagate the hypothetical wavefront with radius of curvature $\tilde{R}_{NIP}$. The corresponding ZO ray with the emergence angle $\tilde{\alpha}$ intersects the first interface at point (x_i, z_i) (Figure 2). The interpolating function that describes the first interface enables to compute the angle of incidence γ_i and the radius of curvature R_F of the interface at point (x_i, z_i).

To continue this ray from the intersection point to the searched-for depth point (x_{21}, z_{21}) of the second interface we require the emergence angle γ_t, given by Snell's law:

$$\frac{\sin \gamma_i}{\sin \gamma_t} = \frac{v_0}{v_1} \,. \tag{4}$$

In addition, we observe that the refracted wavefront focuses at (x_{21}, z_{21}) at the remaining time $t_2/2 - d_1/v_0$:

$$R_T = v_1(t_2/2 - d_1/v_0) \tag{5}$$

Here, R_T denotes the radius of wavefront curvature on the refracted side at the intersection point and d_1 is the distance between the point $(x_0, 0)$ and the point of

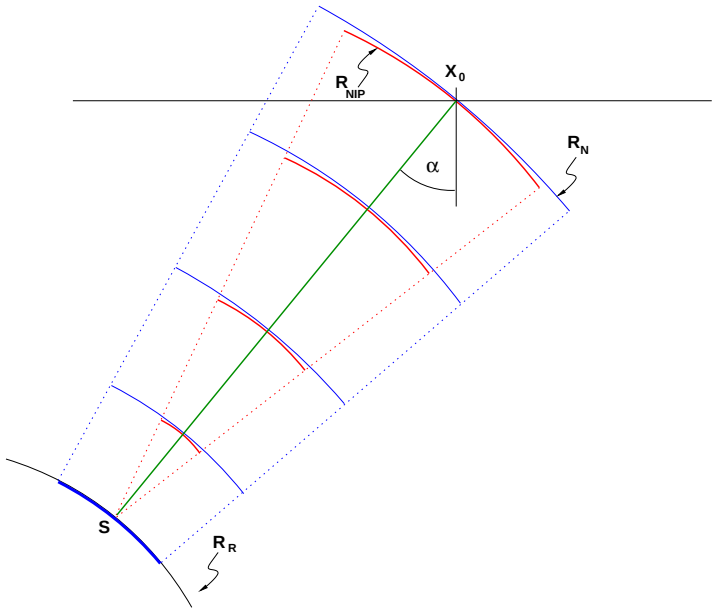

Figure 1: Use of the propagation law to determine a depth point S of the first interface and its radius of curvature R_R at S.

intersection(x_i, z_i). Since the velocity v_1 of the second layer and R_T are not yet known we make use of the refraction law for curved interfaces (Hubral and Krey, 1980):

$$\frac{1}{R_T} = \frac{v_0 \cos^2 \gamma_i}{v_1 R_I \cos^2 \gamma_t} + \frac{1}{R_F \cos^2 \gamma_t}\left(\frac{v_1}{v_0}\cos \gamma_i - \cos \gamma_t\right), \tag{6}$$

where $R_I = \tilde{R}_{NIP} - d_1$ denotes the radius of curvature of the incident wavefront at the point of intersection. These three unknown variables R_T, v_1, and γ_t are determined by solving the three equations (4)-(6) (see Appendix A).

With the knowledge of these parameters, we can propagate the hypothetical wavefronts in the second layer. For the reflection event $P_2 = (x_0, t_2)$, the propagation of the wavefront with radius of curvature $\tilde{R}_{NIP}$ through the first layer focuses after the refraction at the searched-for depth point (x_{21}, z_{21}). The propagation of the wavefront with the radius of curvature $\tilde{R}_N$ yields the curvature of the second interface at depth point (x_{21}, z_{21}).

For every point on a reflection event we receive a depth point and a velocity of the over-lain layer. These velocities are averaged to compute a constant velocity for this layer.

Using the propagation and the refraction law for the hypothetical wavefronts associated with the successive reflection events allows us to establish the whole macro-velocity model. For this inversion procedure as well as for the construction of the

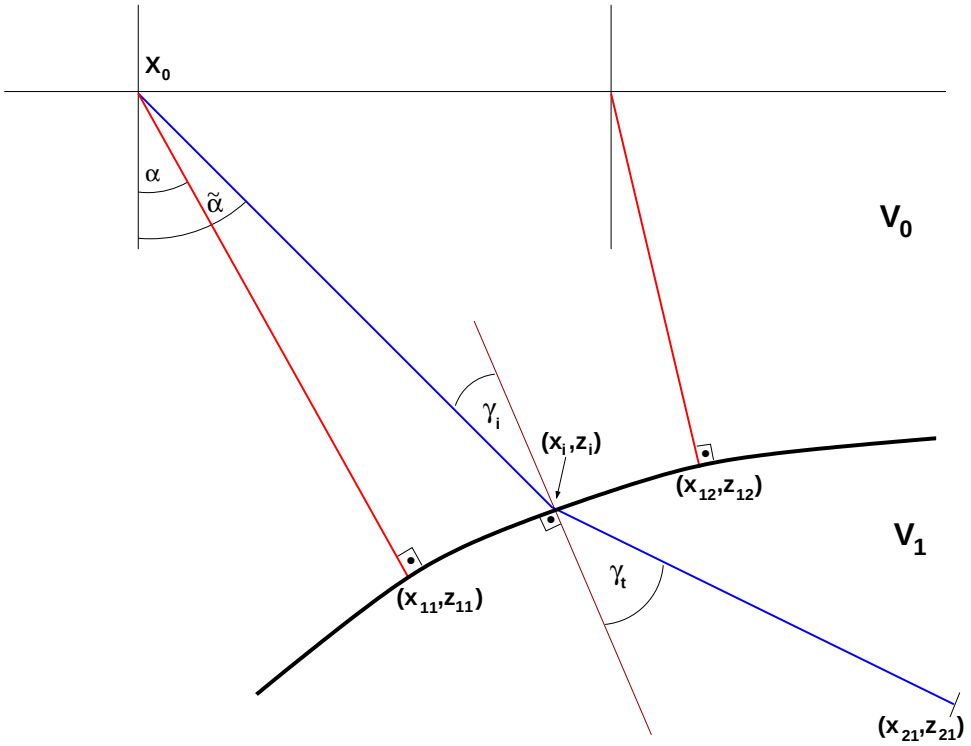

Figure 2: Determination of the point (x_{21}, z_{21}) belonging to the second interface.

interface we do not need to consider the values of R_N. However, R_N can be used to refine the local curvatures of the interfaces.

CONSTRUCTION OF THE INTERFACES

In this section, we present an approach to construct the searched-for interface by means of depth points that belong to the same reflection event. We accentuate that at every depth point (x_{kj}, z_{kj}) first and second derivatives for the interpolating functions are given by the fact that:

- every point (x_{kj}, z_{kj}) of the k^{th}-interface is a normal incident point (NIP) and therefore determines the slope m_{kj} of the interface at (x_{kj}, z_{kj}).
- the propagation of the hypothetical wavefront with radius R_N from x_0 on the surface to depth point (x_{kj}, z_{kj}) yields the radius of curvature R_{kj} of the interface at (x_{kj}, z_{kj}).

To construct an interface we neglect the radii of curvature R_{kj} but make use of m_{kj} as the first derivative of the searched-for interpolating function.

Since the inversion algorithm requires the radius of curvature at any interface point within the interval, the interpolating function has to be at least of second order. To account for the continuity of the second derivative between neighboring segments we actually use third order functions.

Cubic spline interpolation

The goal of cubic spline interpolation is to get an interpolation formula that is smooth in the first derivative and continuous in the second derivative. Since the first derivatives are given by m_{kj} we only require two neighboring points to determine a spline segment. The spline segment between (x_{kj}, z_{kj}) and $(x_{k(j+1)}, z_{k(j+1)})$ is given by

$$z = a_0 + a_1(x - x_{kj}) + a_2(x - x_{kj})^2 + a_3(x - x_{kj})^3 \,.$$

The coefficients have to satisfy the linear equation

$$\begin{pmatrix} 1 & 0 & 0 & 0 \\ 0 & 1 & 0 & 0 \\ 1 & x_{k(j+1)} - x_{kj} & (x_{k(j+1)} - x_{kj})^2 & (x_{k(j+1)} - x_{kj})^3 \\ 0 & 1 & 2(x_{k(j+1)} - x_{kj}) & 3(x_{k(j+1)} - x_{kj})^2 \end{pmatrix} \begin{pmatrix} a_0 \\ a_1 \\ a_2 \\ a_3 \end{pmatrix} = \begin{pmatrix} z_{kj} \\ m_{kj} \\ z_{k(j+1)} \\ m_{k(j+1)} \end{pmatrix}$$

with

$$m_{kj} = \left.\frac{dz}{dx}\right|_{x_{kj}} \qquad \text{and} \qquad m_{k(j+1)} = \left.\frac{dz}{dx}\right|_{x_{k(j+1)}} \,.$$

SYNTHETIC DATA EXAMPLE

For demonstration purposes, we simulated reflections from the interfaces using the ray method to obtain the ZO traveltimes for different models. In addition, we calculated the propagation of the hypothetical wavefronts to determine R_{NIP} and R_N. The emergence angle α is given by the zero-offset ray at the surface.

Dome model

The first model consists of three layers with constant velocities (Figure 3). The first reflector is approximately horizontal with small curvatures over-lain by a layer with velocity $v_0 = 1.5$ km/s. This velocity is used for the inversion algorithm. The second interface is a curved dome-like reflector over-lain by the layer with velocity $v_1 = 4.5$ km/s.

The interfaces, obtained by the inversion algorithm, approximate very well the model interfaces. Figures 4 and 5 illustrate the rays computed for the determination of the second interface. The constructed macro velocity model shows only small

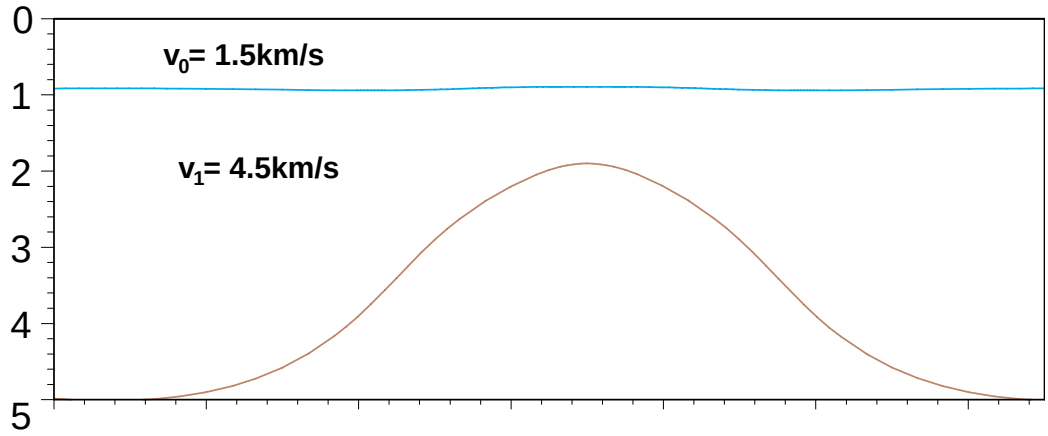

Figure 3: Three layer model with constant velocities.

variation compared to the model (see Figure 5). We obtained an average velocity of $v_1 = 4.50$ km/s for the second layer, with a standard deviation of $\sigma = 0.14$ km/s.

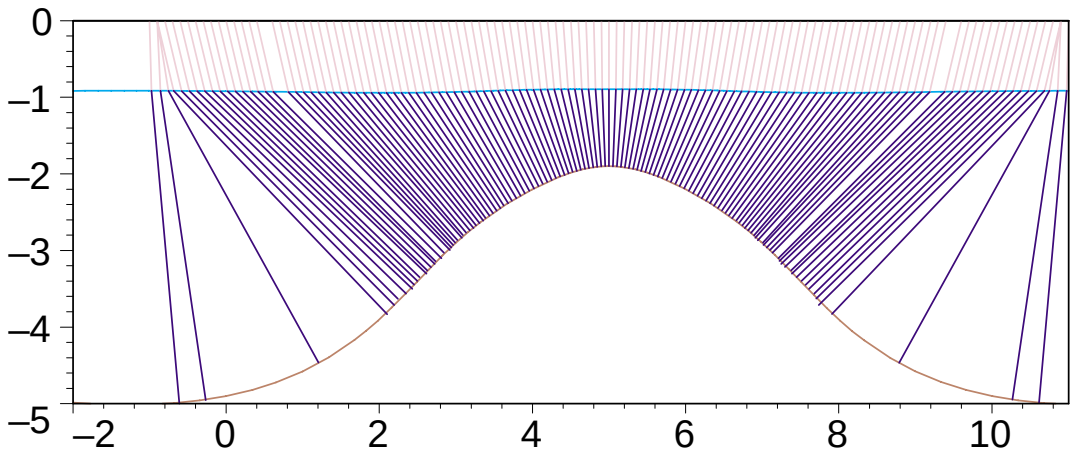

Figure 4: Depth model obtained from the inversion procedure and the original model. The endpoints of the rays illustrate the computed depth points for the second interface.

Syncline Model

Like for the dome model, we constructed a three layer model with a syncline interface. The velocities are $v_0 = 1.5$ km/s for the near surface layer and $v_1 = 3.8$ km/s for the second layer (Figure 6).

The first circular reflector has the constant radius of curvature $R_F = 23.8$ km. The computations yield an accurate first interface while the endpoints of the rays for the

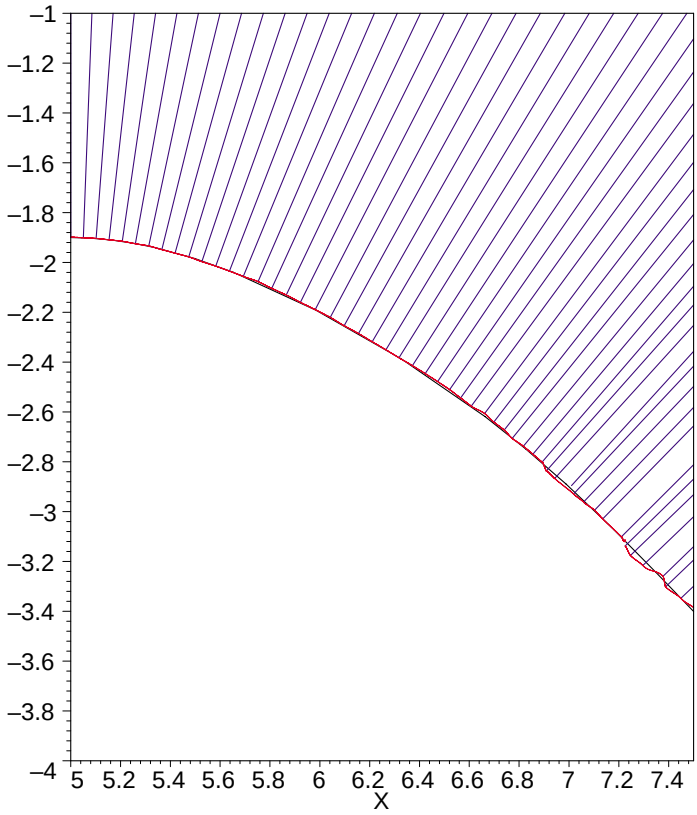

Figure 5: Detail of Figure 4.

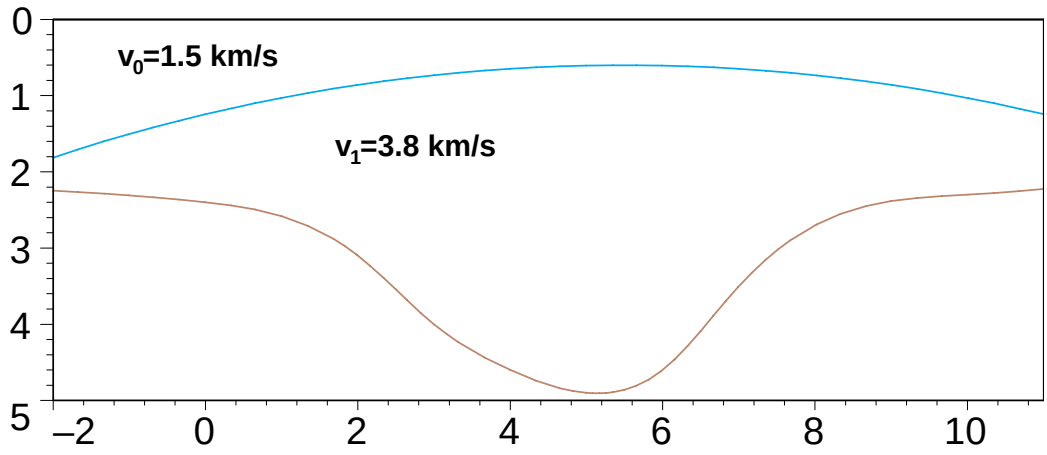

Figure 6: Three layer model with constant velocities and constant curvature for the first interface.

second interface are slightly scattered around the model interface (see Figures 7 and 8). This is due to the fluctuations of determined radii of curvatures R_F. Such a result would require smoothing of the computed radii. Using the given constant curvature for the first interface in formula (A-5), we obtained depth points in good agreement with the model (see Figures 9 and 10) We calculated for the spline interpolation an average velocity of $v_1 = 3.80$ km/s for the second layer, with a standard deviation of $\sigma = 0.47$ km/s.

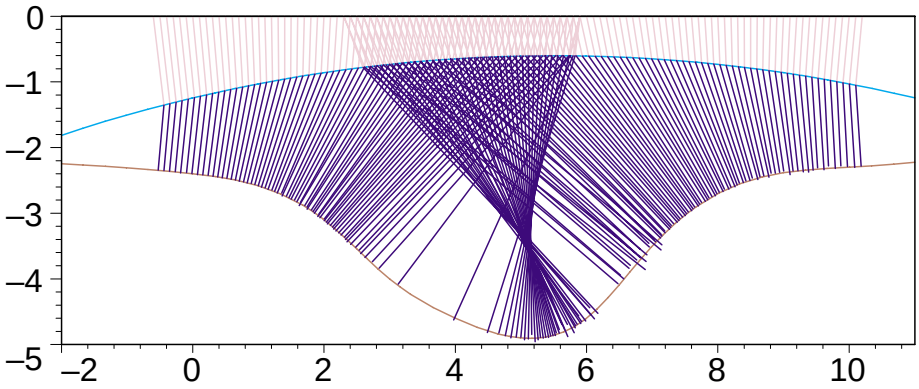

Figure 7: Zero-offset rays to the depth points.

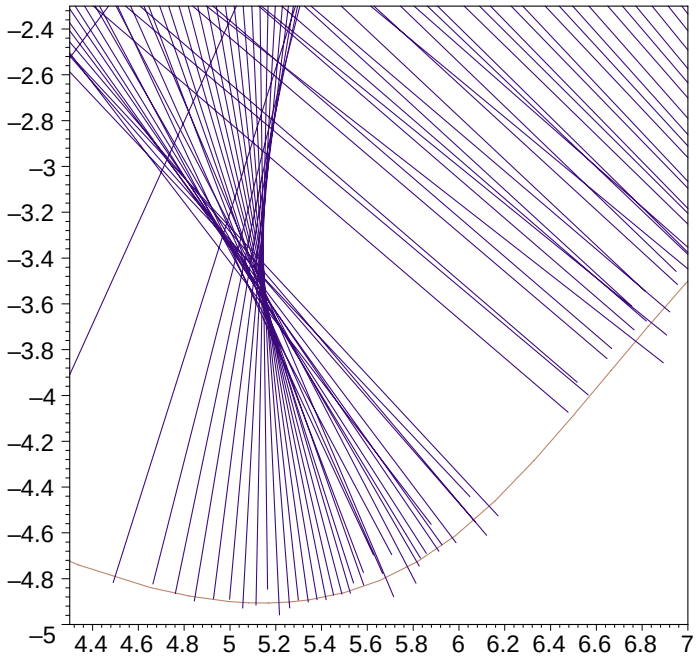

Figure 8: Detail of Figure 7.

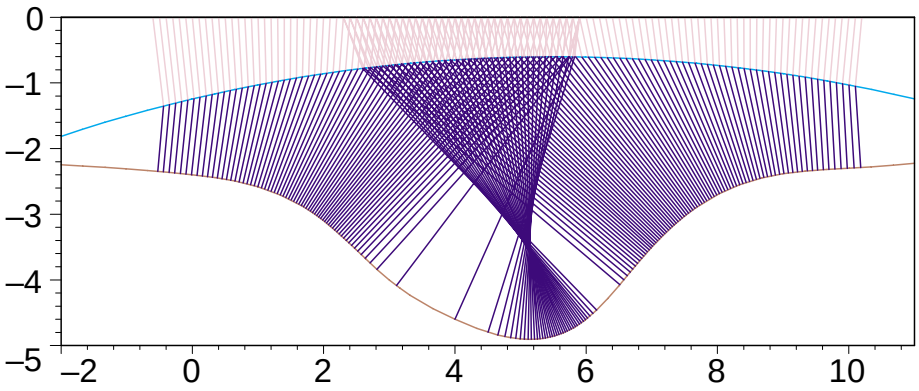

Figure 9: Zero-offset rays to the depth points. Inversion based on the known constant curvature of the first interface.

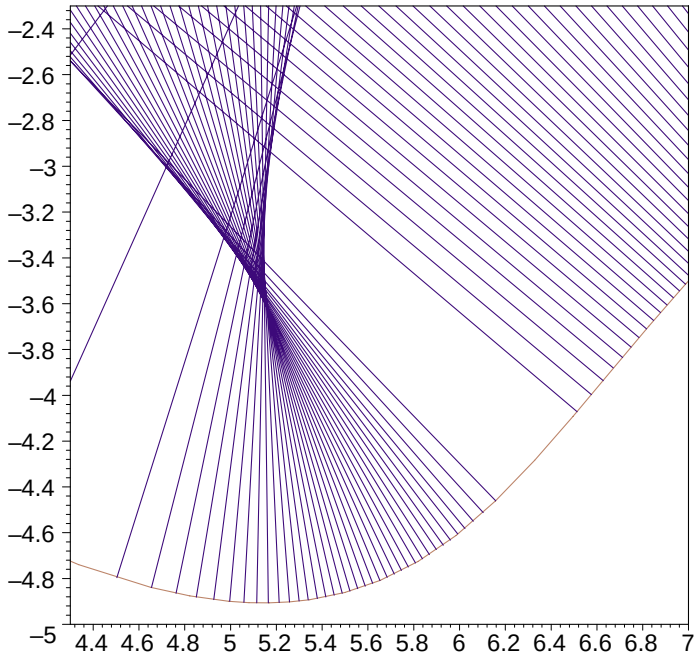

Figure 10: Detail of Figure 9.

CONCLUSION

We presented an inversion algorithm to determine a macro-velocity model from zero-offset primary reflection events and associated wavefield attributes. The procedure uses only R_{NIP} and α and interpolating functions of third order to represent the interfaces and to perform the layer stripping. The results of the inversion procedure match the models very well. Thus, the inversion algorithm itself works perfectly in an analytical point of view. It only lacks sometimes due to numerical problems. As we have shown in the second example, the formula (A-5) is very sensitive on fluctuations of R_F, the radii of curvatures of the interfaces. Consequently, one has to smooth the radius R_F along the interface by using other approximating functions, e. g. approximating cubic splines with free knots for an interval of depth points.

REFERENCES

de Bazelaire, E., Höcht, G., Majer, P., and Hubral, P., 1999, Seismics and optics — hyperbolae and curvatures: 61th Mtg. Eur. Assoc. Expl. Geophys., Extended Abstracts.

Höcht, G., Mann, J., and Jäger, R., 1999, The common reflection surface stack - Part I: Theory: Wave Inversion Technology consortium, annual report, pages 7–23.

Hubral, P., and Krey, T., 1980, Interval velocities from seismic reflection traveltime measurements: Soc. Expl. Geophys.

Hubral, P., 1983, Computing true amplitude reflections in a laterally inhomogeneous earth: Geophysics, **48**, no. 08, 1051–1062.

Jäger, R., Mann, J., and Höcht, G., 1999, The common reflection surface stack - Part II: Application: Wave Inversion Technology consortium, annual report, pages 25–46.

Nürnberger, G., 1989, Approximation by spline functions: Springer Verlag.

Press, W., Teukolsky, S., Vetterling, W., and Flannery, B., 1992, Numerical recipes in C: Cambridge University Press.

APPENDIX A

Solving the equations (4)-(6) yields

$$R_T = \frac{A}{2}(t_2 v_0 - 2d_1), \tag{A-1}$$

$$v_1 = A v_0, \tag{A-2}$$

$$\sin\gamma_t = A \sin\gamma_i\,. \tag{A-3}$$

with the solutions of the fourth order polynom in **Z**:

$$\begin{aligned}
A &= [\cos^4\gamma_i R_F^2 t_2^2 v_0^2 + 2\cos^3\gamma_i R_F t_2^2 v_0^2 R_T - 8\cos^3\gamma_i R_F t_2 v_0 R_T d_1 \\
&+ 8\cos^3\gamma_i R_F d_1^2 R_T + (1-\cos^2\gamma_i) R_T^2 t_2^2 v_0^2 - 4(1-\cos^2\gamma_i) R_T^2 t_2 v_0 d_1 \\
&+ 4R_T^2 R_F (1-\cos^2\gamma_i)\cos\gamma_i t_2 v_0 - 8R_T^2 R_F (1-\cos^2\gamma_i)\cos\gamma_i d_1 \\
&+ R_T^2\cos^2\gamma_i t_2^2 v_0^2 + 4\cos^4\gamma_i R_F^2 d_1^2 + 4R_T^2 R_F^2 (1-\cos^2\gamma_i)^2 + 4R_T^2\cos^2\gamma_i d_1^2 \\
&- 4\cos^4\gamma_i R_F^2 t_2 v_0 d_1 - 8\cos^2\gamma_i R_F^2 d_1 R_T (1-\cos^2\gamma_i) + 4(1-\cos^2\gamma_i) R_T^2 d_1^2 \\
&+ 4\cos^2\gamma_i R_F^2 t_2 v_0 R_T (1-\cos^2\gamma_i) - 4R_T^2\cos^2\gamma_i t_2 v_0 d_1]\mathbf{Z^4} \\
&- 8R_T^2 R_F^2 (1-\cos^2\gamma_i) - 4R_T^2 d_1^2 + 8R_T^2 R_F\cos\gamma_i d_1 + 8\cos^2\gamma_i R_F^2 d_1 R_T \\
&+ [4R_T^2 t_2 v_0 d_1 - R_T^2 t_2^2 v_0^2 - 4\cos^2\gamma_i R_F^2 t_2 v_0 R_T - 4R_T^2 R_F\cos\gamma_i t_2 v_0]\mathbf{Z^2} \\
&+ 4R_T^2 R_F^2.
\end{aligned} \tag{A-4}$$

Equation (A-4) gives four possible solutions, but due to physical constraints they reduce to one single solution:

$$\begin{aligned}
A &= 1/2(R_T t_2^2 v_0^2 - 4R_T t_2 v_0 d_1 + 4\cos^2\gamma_i R_F^2 t_2 v_0 + 4R_T R_F\cos\gamma_i t_2 v_0 \\
&+ 8R_T R_F^2 - 8R_T R_F^2\cos^2\gamma_i + 4R_T d_1^2 - 8R_T R_F\cos\gamma_i d_1 - 8\cos^2\gamma_i R_F^2 d_1 \\
&- R_F((24R_T^2 t_2^2 v_0^2 d_1^2 - 8R_T^2 t_2^3 v_0^3 d_1 - 32R_T^2 t_2 v_0 d_1^3 - 64R_T^2 d_1^3 R_F\cos\gamma_i \\
&- 64R_T d_1^3\cos^2\gamma_i R_F^2 + 16R_T^2 d_1^4 + R_T^2 t_2^4 v_0^4 - 48R_T^2 t_2^2 v_0^2 R_F\cos\gamma_i d_1 \\
&- 48R_T t_2^2 v_0^2\cos^2\gamma_i R_F^2 d_1 + 96R_T^2 t_2 v_0 d_1^2 R_F\cos\gamma_i + 96R_T t_2 v_0 d_1^2\cos^2\gamma_i R_F^2 \\
&+ 8R_T t_2^3 v_0^3\cos^2\gamma_i R_F^2 + 8R_T^2 t_2^3 v_0^3 R_F\cos\gamma_i)/R_F^2)^{1/2}) R_T/(4R_T^2 R_F^2 \\
&+ \cos^4\gamma_i R_F^2 t_2^2 v_0^2 + 4R_T^2 R_F^2\cos^4\gamma_i + 8\cos^3\gamma_i R_F d_1^2 R_T - 4R_T^2 R_F\cos^3\gamma_i t_2 v_0 \\
&- 4\cos^4\gamma_i R_F^2 t_2 v_0 R_T - 4R_T^2 t_2 v_0 d_1 + 8R_T^2 R_F\cos^3\gamma_i d_1 + 8\cos^4\gamma_i R_F^2 d_1 R_T \\
&- 8R_T^2 R_F^2\cos^2\gamma_i - 4\cos^4\gamma_i R_F^2 t_2 v_0 d_1 - 8\cos^3\gamma_i R_F t_2 v_0 R_T d_1 \\
&+ 2\cos^3\gamma_i R_F t_2^2 v_0^2 R_T - 8\cos^2\gamma_i R_F^2 d_1 R_T - 8R_T^2 R_F\cos\gamma_i d_1 + 4R_T^2 d_1^2 \\
&+ 4\cos^2\gamma_i R_F^2 t_2 v_0 R_T + 4R_T^2 R_F\cos\gamma_i t_2 v_0 + R_T^2 t_2^2 v_0^2 + 4\cos^4\gamma_i R_F^2 d_1^2).
\end{aligned} \tag{A-5}$$